Ruprecht-Karls-University Heidelberg
Faculty for Life Sciences
Molecular Biotechnology

Identification of thyroid cancer subtypes driving carcinogenesis through different ways of proliferative signaling

Data Science Project SoSe 2022

Authors   Anna Lange, David Matuschek, Jakob Then, Maren Schneider
Date   20.07.2022

Abstract

In recent years bioinformatic methods became a tool of utmost importance in medical research. To detect specific gene and pathway patterns in different cancer types or histological types, here, we perform pan-cancer analysis. Furthermore, we carry out a focused analysis to specify different subcategories within a certain cancer type and to identify targets for therapy. As main methods in identifying up- or downregulated pathways, Gene Set Enrichment Analysis (GSEA) and Gene Set Variation Analysis (GSVA) are used. GSVA of The Cancer Genome Atlas (TCGA) expression data, containing 33 different tumor types, reveals four clusters of cancer types, which are defined by different histological types like glioblastoma and adenocarcinoma. Thus, the histological types seem to correlate with a specific set of pathways that are especially enriched in certain types. Furthermore, GSVA results of Thyroid cancer (THCA) expression data show that thyroid carcinogenesis is associated with the upregulation of proliferation signaling pathways like the hedgehog pathway, alpha6beta4 integrin signaling pathway, and associated pathways such as interleukin 36 signaling. Based on those proliferation signaling pathways, three subclusters form inside the THCA patients from the pan-cancer data. One THCA subcluster could be linked to the follicular histological subtype and is defined by increased mTOR and MAPK activity while having low alpha6beta4 activity. In contrast, another THCA subcluster is defined by a low mTOR and MAPK activity, but a high alpha6beta4 activity. The third THCA subtype we identified shows both ways of proliferation signaling. These results promise more success in THCA treatment, as a more precise diagnosis of the distinct THCA subtypes is possible allowing for better treatment. To improve the understanding of THCA, and thereby bettering patients' prognosis, this project focuses on finding genes that have a significantly altered expression in THCA compared to other cancers and especially to normal tissue.

Abbreviations

BRCA – Breast invasive carcinoma

EGFR – Endothelial growth factor receptor

ERBB2 – Erb-b2 receptor tyrosine kinase 2

EWSR1/FLI1 – Ewing sarcoma breakpoint region 1 / Friend leukemia integration 1

FTC – Follicular thyroid cancer

GSEA – Gene Set Enrichment Analysis

GSVA – Gene Set Variation Analysis

IL-36 – Interleukin 36

JAK/STAT – Januskinase / Signal Transducers and Activators of Transcription

KICH – Kidney renal papillary cell carcinoma

KIRC – Kidney renal clear cell carcinoma

LIHC – Liver hepatocellular carcinoma

Log2FC – Log2 fold change

LUAD – Lung adenocarcinoma

MAPK – Mitogen-activated protein kinase

MSE – Mean squared error

MST1 – Makrophage stimulating protein 1

mTOR – Mammalian target of rapamycin

NF-kB – Nuclear factor kappa-light-chain-enhancer of activated B-cells

PCA – Principal component analysis

PI3K – Phosphoinositid-3-kinase

PRAD – Prostate adenocarcinoma

PTC – Papillary thyroid cancer

RAS – Rat sarcoma

TCGA – The Cancer Genome Atlas

TCV – Tall cell variant

THCA – Thyroid carcinoma

UMAP – Uniform manifold approximation and projection

UTC – Undifferentiated thyroid cancer

UVM – Uveal melanoma

Contents

1 Introduction

In 2019 230,000 cancer deaths were documented in Germany[1]. To detect and fight these tumors, the development of new treatment and detection methods is essential. A crucial step in this direction was the definition of the Hallmarks of Cancer - properties present in every tumor (Hanahan and Weinberg, 2011). However, the different histological types of tumors are equally important when characterizing cancers. Carcinoma, which can be further subcategorized into adenocarcinoma, squamous cell carcinoma, and transitional cell carcinoma, all derive from epithelial cells. Further forms include melanomas, glioblastomas and leukemia (Alberts and Walter, 2015).

Here we focus on thyroid carcinoma (THCA) as its incidence increased dramatically over the past few years (Cabanillas *et al.*, 2016). Papillary thyroid cancer (PTC), follicular thyroid cancer (FTC), and a tall cell variant (TCV) are subtypes of differentiated thyroid cancer. Among them DTCs and PTCs have the best clinical prognosis (Lin, 2007), while TCV cancers have the worst outcome (Coca-Pelaz *et al.*, 2020). Therefore, the characterization of different or distinct expression patterns for each histological subtype would be important for more specific therapy options (Kant *et al.*, 2020). For example, only some THCAs subtypes experience integrin alpha6beta4 driven carcinogenesis which might provide a viable target for therapy. Integrins are cellular adhesion molecules, that bind to laminin in the extracellular matrix (Liberzon *et al.*, 2015a). Alterations of integrin signaling are very common in cancer cells (Rabinovitz and Mercurio, 1996).

To analyze how the activity of a gene set differs between two sets of gene expression data, a Gene Set Enrichment Analysis (GSEA) is performed. For this, the genes in the expression data have to be ranked decreasingly by a certain metric like the associated p-values or the log2 fold change. After ranking, a cumulative sum of all expression values in the ranked sample is computed. If a gene is present in the gene set to be analyzed the expression value of that gene is added to the running sum, otherwise it is subtracted. The extremum of this running sum is termed the enrichment score of the gene set. (Subramanian *et al.*, 2005)

The Gene Set Variation Analysis (GSVA) is performed with the same intention as the GSEA. However, no reference data is required to successfully perform GSVA. GSVA is performed in following five steps. First, the cumulative density distribution of a gene over all samples is estimated. Then the expression statistic of a gene in a sample is calculated based on the cumulative density distribution to bring all of the expression values to the same level. The third step is to rank the genes based on the expression statistic and to normalize the ranks with z-transformation. Lastly, the enrichment score is computed based on the obtained ranked list by calculating the Kolmogorov-Smirnov-like rank statistic for each gene set. (Hänzelmann *et al.*, 2013a)

The Uniform manifold approximation and projection for dimension reduction (UMAP) is a fast method to reduce the dimension of a multidimensional data set while preserving the global structure of the data (Maaten and Hinton, 2008). The algorithm starts by setting up a high-dimensional graph representation of the data. From each data point, a radius is extended and when two radii come into contact the points are connected in the graph. The algorithm goes on until k points are connected

---

[1]https://www.krebsinformationsdienst.de/tumorarten/grundlagen/krebsstatistiken.php

or n iterations are reached. The resulting clustered high-dimensional graph is then optimized for visualization in low dimensions. However, this non-linear dimension reduction results in the distances between individual points not being proportional to their real distance. (Sharma *et al.*, 2021)

For data regression, a neuronal network can be used. In general, a deep learning network consists of an input layer, multiple hidden layers, and an output layer consisting of various neurons (Riedmiller). The number of neurons in each hidden layer and the number of hidden layers vary and must be tested to give the best results. The activation of each neuron can be described as a linear composition of all the inputs x_i from the previous layer associated with a weight w_i and a bias b_i:

$$Activation = \sum_{i=1}^{n} w_i x_i + b_i$$

The "learning effect" of the network is achieved by optimizing the randomly chosen weights and biases via gradient descent. To do so, for each training iteration the error of the network is computed by a cost function. Next, the cost function value must be reduced. Therefore, its gradient is computed, and all weights and biases are adjusted accordingly in a process called backpropagation. For the next samples, those steps are repeated to reach the minimum of the cost function. A drawback of this method is that gradient descent only identifies local minima of the cost function. To find a global minimum the training has to be repeated with various initial weights and biases.

Using pan-cancer expression data, we identify clusters between cancer types regarding their expression profiles as well as the hallmark and metabolic pathway activities. Then, our focus shifts to THCA, where we discover subclusters in gene expression linking them to histological types. Additionally, we analyze pathways that alter significantly between THCA and homeostatic thyroid tissue and predict their activities with linear and neuronal network regression.

2 Materials and Methods

We were provided with bulk RNA-seq gene expression data and the corresponding clinical annotations from the cancer genome atlas (TCGA). The data was processed and cleaned by workflows described in the supplementary materials section.

2.1 Methods for descriptive analysis

In a mean-variance plot, the variance is plotted over the mean expression value of a single gene across all patients. Thus, the variance and mean were calculated for each gene in the THCA expression data. The final plot was created with the package ggplot2 (Wickham, 2016). A volcano plot is used to identify genes displaying significantly differentially expressed genes in cancerous versus homeostatic tissues. First, the log2 fold change (Log2FC) is calculated for each gene across all samples in the THCA expression data in the following way:

$$log2FC = mean(normaltissue) - mean(tumortissue)$$

Next, a two-sided Wilcoxon rank sum test was performed with the `wilcox.test()` function to determine the significance of a difference in expression. To avoid the accumulation of type one errors, a Bonferroni correction was performed. Genes with a lower p-value than the corrected significance level α are significantly differentially expressed. If the Log2FC is additionally positive, the genes are significantly overexpressed in tumor tissue and vice versa.

2.2 Gene Set Scoring and Dimension Reduction

The GSEA was used to identify enriched pathways in THCA tumor tissue. Here, GSEA was performed with the package "fgsea" (Korotkevich *et al.*, 2019). First, the expression values were ranked in decreasing order by Log2FC for every patient. Log2FC was chosen as the ranking metric as it is easy to compute and shows a high sensitivity (Zyla *et al.*, 2017). Secondly, using the ranked Log2FC vectors, the enrichment score of each pathway was calculated for each patient with the `fgsea::fgseamultilevel()` function.

As no normal tissue reference data was provided for the TCGA expression data, pathway activities were computed via GSVA. The analysis was performed with the `gsva::gsva()` function from the "GSVA" package (Hänzelmann *et al.*, 2013b). To give a general overview of the differences in expression of THCA and homeostatic thyroid tissue GSVA, the THCA expression data were also analyzed by GSVA. To do so, tumor and normal expression data were combined into a singular data frame of which enrichment scores were computed. Then, the GSVA data was split again and the log2FC between the two matrices was computed and taken as pathway activity.

PCA was performed to provide a set of orthogonal data for the subsequent UMAP. For the pancancer GSVA pathway activity data the `prcomp()` function was used. To verify the results, PCA was performed on TCGA expression data, as well. In this case `Seurat::RunPCA()` from the Seurat package was used to minimize computation time (Hao *et al.*, 2021). UMAP analysis was conducted on all principle components from previous PCA to identify and visualize clusters in TCGA GSVA and expression data. This was achieved with the `umap::umap()` function from the package "umap" (Konopka, 2022) running on all PCs from TCGA GSVA expression data.

2.3 Regression analysis

For THCA pathway activity regression analysis a highly variant and significantly altered pathway was selected. To prepare the data appropriately the THCA GSEA data set was divided into a training and test data set containing 44 and 15 samples respectively. A linear regression analysis was performed on the training data with the `glm()` function. To do so, the correlation of all pathways was computed and pathways with high correlations were omitted. Subsequently, 10% of the most variant pathways were selected as variables for the regression model. A second model was introduced by selecting only those pathways contributing significantly to the model.

A neural network was implemented to predict the pathway activity using the `neuralnet()` function from the "neuralnet" package (Fritsch *et al.*, 2019). For identification of the best initial conditions, 25

different networks were generated, each with two hidden layers and different combinations of neurons per layer. For each combination, the network was trained on the min-max-scaled training data, and the best network was determined by the lowest mean squared error (MSE) in the test data.

2.4 Environment

The R version 4.0.1 was used, the table of used packages is attached in the supplementary material (table 6.1).

3 Results

3.1 Preprocessing

Dimension reduction through low-variance and biotype filtering. TCGA genes with a variance lower than 0.1 were removed. The low-variance filtering of the THCA data set was done similarly. Genes with lower variance than 0.06 were deleted in the tumor tissue and the normal tissue data. To reduce dimensionality further, the biotype of the hallmark pathway genes was determined, which was almost exclusively protein-coding. To match this, only protein-coding pathways were kept in all expression data sets for further analysis. In doing so, the number of genes in the pan-caner data set was reduced from 60,000 to approximately 19,000 genes and from approximately 20,000 genes to 15,000 genes in the THCA data.

MSigDB pathway filtering. To test for similarity in the selected metabolic pathways compared to the hallmark pathways and the metabolic pathways themselves, the Jaccard index between all pathways was calculated. Pathways with a high Jaccard indexes were identified and subsequently deleted. The number of MSigDB pathways could thus be reduced from 6366 to 657.

3.2 Descriptive analysis

Mean-variance plot of TCGA expression data shows highly variant genes. To determine the genes from the TCGA expression data with high variance, the variance was plotted over the mean (Supplementary material figure 6.1). The distribution of genes in this plot shows that the highly variant genes are around a log2 mean expression level of 0. The plot also shows that very few genes are at a low or a very high mean expression level. Most genes are expressed across all patients at a log2 mean expression level of approximately 0. Among the most variant genes were RPS4Y, CORNIFIN and CK-6C.

Significantly up- and downregulated genes in THCA obtained from volcano plots. To determine up- or downregulated genes in THCA corresponding p-Values were computed with a Wilcoxon rank sum test. (Figure 3.1). The significance level was adjusted to 1.755e-06 with a Bonferroni adjustment.
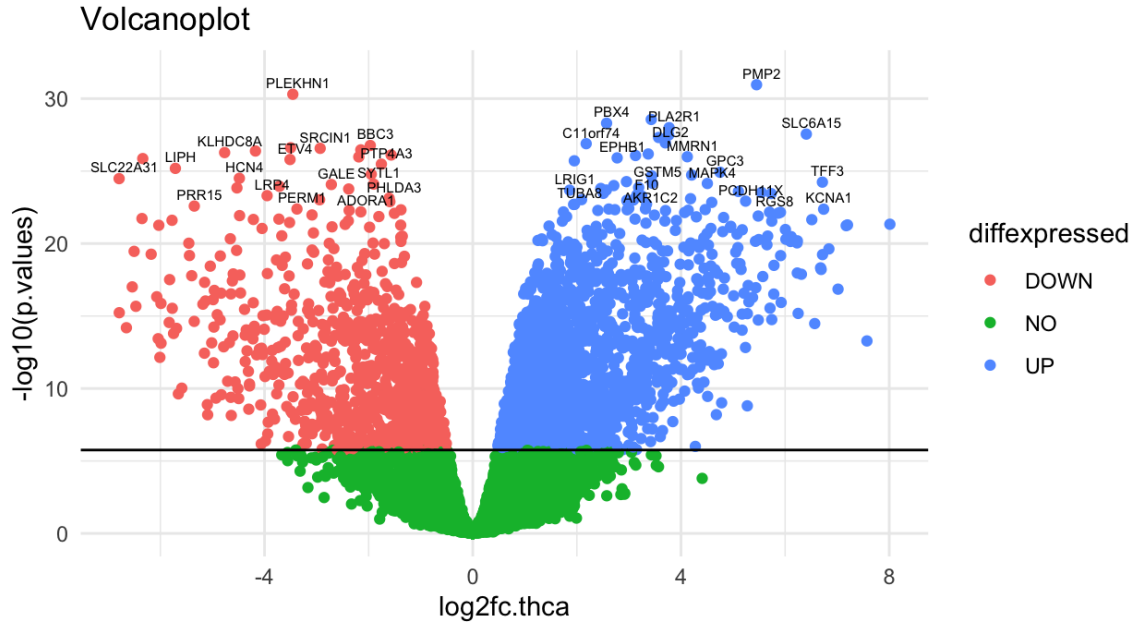
Figure 3.1: Volcano plot of THCA expression data. Downregulated genes are colored red, upregulated genes blue. Not significantly altered genes are colored green. Most significantly altered genes are labelled with their gene symbol

3.3 Pan cancer analysis

GSVA of TCGA expression data reveals four clusters of cancer types. A pathway activity matrix was computed as described in methods section. The obtained pathway activity matrix was visualized as a heatmap. (Figure 3.2 and supplementary material figure 6.3) The tumor types were clustered hierarchically based on their mean pathway activity and formed four clusters correlating with their histological type. The first cluster contains mainly adenocarcinomas, while the second one contains predominately glioblastomas. Leukemias are found only in the third cluster, and the last cluster is enriched with sarcomas and carcinomas. Melanomas appear in the second and fourth clusters. Furthermore, three observations were made regarding specific information about pathway activity. Pathways, which are important for nucleus import and export like the Ran shuttle pathway, as well as pathways for transcription regulators in embryonic stem cells are downregulated in glioblastoma and adenocarcinoma. However, these pathways are upregulated in all other histological types. Another observation is the clustering of glioblastoma. Pathways initiating neurogenesis and pathways linked to differentiation of the neural crest are upregulated only in glioblastoma (Wang *et al.*, 2021). Two other pathways, that are upregulated in glioblastoma cells are pathways linked to the activity of tyrosine kinases. The upregulation of tyrosine kinases promotes cell growth and proliferation (Alberts and Walter, 2015). Taken together these two observations are in line with the expected high proliferation rate commonly found in glioblastoma. The third cluster is mainly related to adenocarcinomas, more specifically liver hepatocellular carcinoma (LIHC), kidney renal papillary cell carcinoma (KICH) and kidney renal clear cell carcinoma (KIRC). The upregulated pathways are involved in the metabolism of carbohydrates, synthesis of lipids, synthesis of amino acids and detoxification.
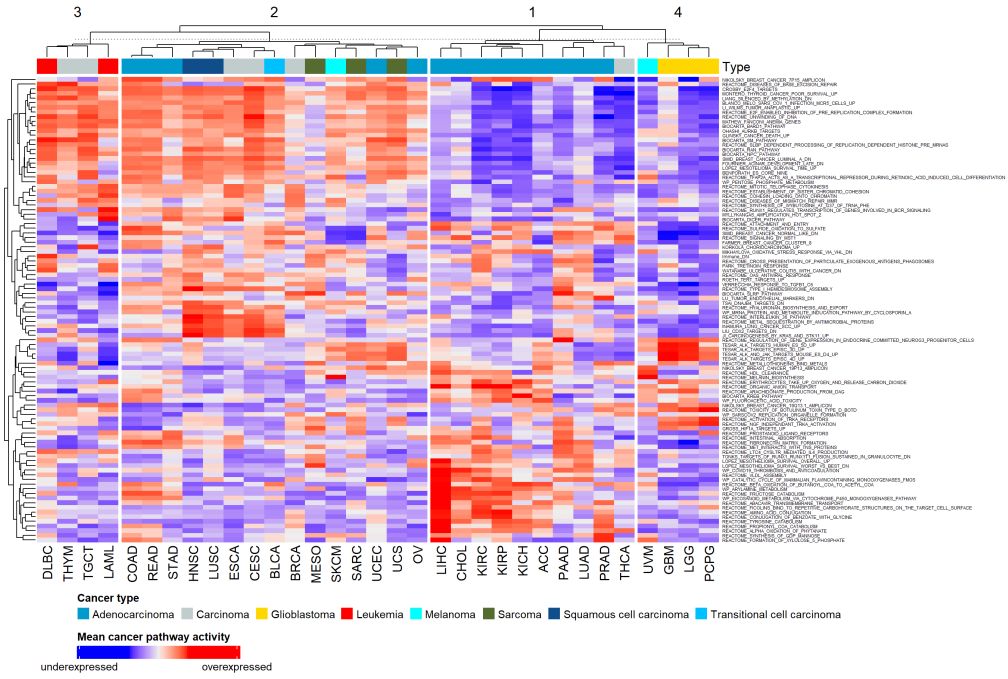
Figure 3.2: Mean pathway activity of the 100 most variant pathways for each tumor type. Column clusters were obtained by complete hierachical clustering and subsequently split into four groups. Pathway activities were computed via GSVA of pan-cancer expression data. For all sample activities see figure 6.3.

Dimension reduction of GSVA pan-cancer data reveals clusters in pathway activity. PCA was performed on GSVA pan-cancer data for UMAP analysis. No apparent clustering was observed in the PCA data. Subsequent UMAP analysis, showed clear clusters for most cancer types. (Figure 3.3 and supplementary material figure 6.2). This complements the results obtained from our heatmap and reassures, that the tumor types have characteristic pathway activities. However, some cancers clustered better with their histological type rather than tumor type. This was observed mainly for carcinomas like squamous cell carcinoma and transitional cell carcinoma, as well as sarcoma, lung adenocarcinoma, and ovarian cancer. These are the same histological types that proved difficult to cluster in the mean GSVA of TCGA expression. The UMAP confirmes, that the histological type of a tumor has a major impact on the patients' gene expression profile. The same analysis was performed for gene expression activity instead of pathway activity to check for the reliability of the results. Similar clusters were observed, which confirms our results.

3.4 Focused analysis

GSVA on THCA expression data reveals pathways driving thyroid carcinogenesis. To grasp a general overview of the differences in pathway activity between THCA and homeostatic thyroid tissue, GSVA was performed for the THCA expression data. Based on the GSVA results, altered pathways were identified using the workflow described for volcano plots 3.4. Most prominently among them were pathways linked to proliferative signaling, such as upregulation of p53 inhibitory proteins and hedgehog pathway activating Gli proteins. Further, the alpha6beta4 integrin signaling pathway
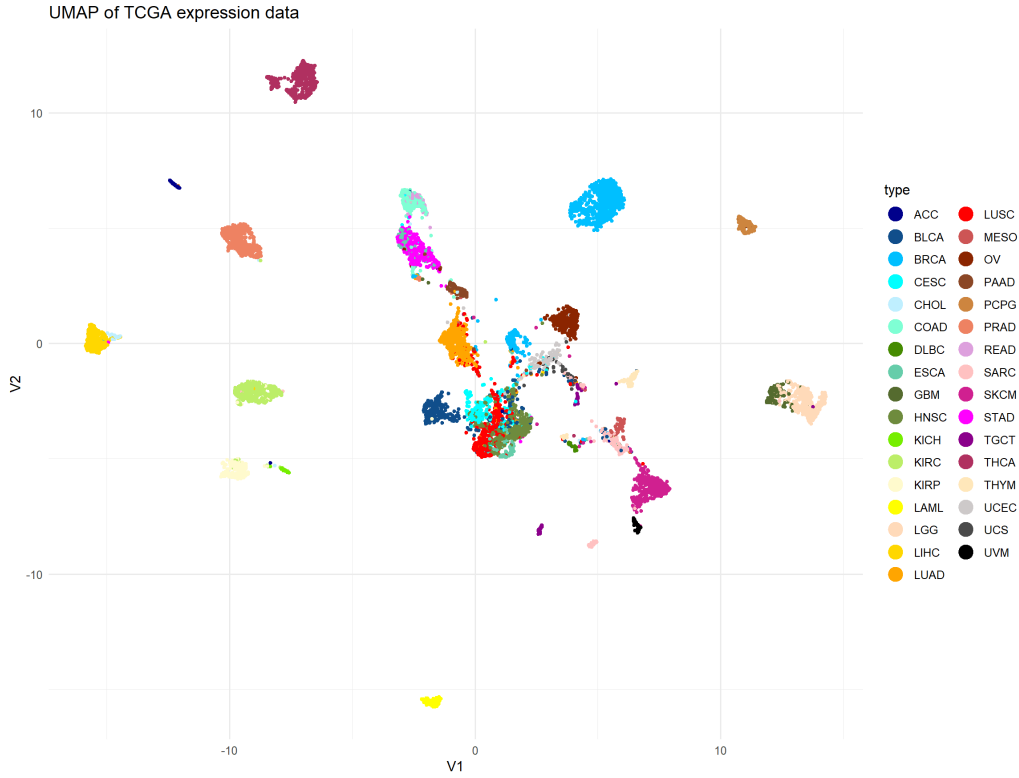
Figure 3.3: UMAP of TCGA pathway activity. Data points are colored by tumor type

and associated pathways such as IL-36 signaling and Typ I hemidesmosome synthesis were significantly enhanced in THCA. Further, signaling through the EWSR1/FLI1-fusion protein was upregulated significantly. Lastly, THCA showed downregulation of non-histone protein methylation.

Pan-cancer data GSVA reveals three subtypes of THCA altering in proliferative signaling.
To investigate potential subtypes of THCA, the respective samples were taken from the pan-cancer GSVA data. The optimal number of clusters was determined by an elbow plot and subsequent k-means clustering revealed a total of three subtypes in THCA (Figure 3.5). This is consistent with the three clusters of THCA observed in the full pan-cancer GSVA data. The follicular histological type was enriched in cluster B, with no tall cell types present in this cluster. Judging from histological type alone no difference in clusters A and C was observed. Most significant changes in pathway activity were observed in pathways concerning proliferative signaling. In comparison with all other tumor types, cluster A displayed high activity of RAS, JAK/STAT and EWSR1/FL1-fusion mediated signaling as well as elevated signatures associated with carcinogenesis driven by alpha6beta4 activity. In contrast, these pathways were downregulated in cluster B, with it showing elevated activity in mTOR, MAPK, PI3K, and EGFR signaling cascades. Cluster C was found to upregulate all the aforementioned forms of proliferative signaling. All clusters showed a homogenous upregulation of hedgehog, ERBB2, and MST1 pathway activity. Regarding immune response, cluster C showed no significant alterations in the respective hallmark pathways, however, these pathways were downregulated in both clusters A and B. With this data, we can identify two seemingly different forms of proliferative signaling driving carcinogenesis in THCA. These forms can either occur separately as in the case of clusters A and B or combined as for cluster C.

Figure 3.4: Volcano plot of THCA pathway activity. Downregulated pathways are colored red, upregulated pathways blue. Not significantly altered pathways are colored green. Most significantly altered pathways are labelled with their name.
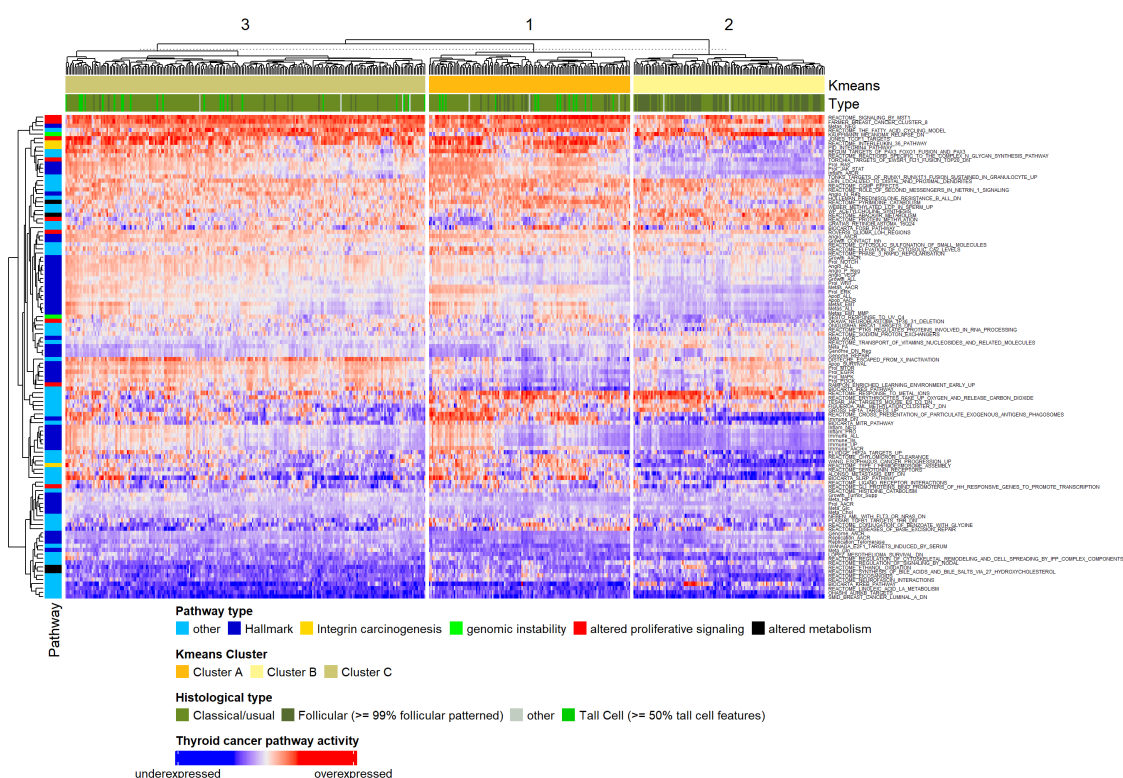

Figure 3.5: Pathway activity of the 50 most variant, hallmark, and 20 most significantly altered pathways for each patient. Column clusters were obtained by k-means clustering with k=3. Pathway activities were computed via GSVA of pan-cancer expression data.

THCA subtypes do not differ in their metabolism. To investigate how the identified subtypes compare to homeostatic thyroid tissue, GSEA was performed for the THCA data. Consistent with the pan-cancer analysis of THCA data, k-means clustering obtained three different clusters in pathway activity – verified as the optimal number of clusters via an elbow plot. All clusters showed a similar change in metabolism (Supplementary material figure 6.4). Catabolic pathways are downregulated whereas anabolic pathways e.g., fatty acid synthesis show increased activity in comparison with normal tissue. Further, the results seem consistent with the proliferative signaling activities found previously. Alpha6beta4, RAS, JAK/STAT, and EWSR1/FL1-fusion mediated signaling is upregulated in clusters one and three with low expression in cluster two. However, the upregulation of mTOR, MAPK, PI3K, and EGFR signaling in clusters two and three was observed only in some samples. Regarding, immune response the expression profiles are again consistent with differences observed in the GSVA pan-cancer data: Both clusters one and two show a lower immune response compared to cluster three. From these GSEA results, we can conclude that the three subtypes of THCA differ in carcinogenesis and associated immune response but share a similar metabolism consistent with the Warburg effect.

3.5 Regression analysis of THCA pathway activity

To select a suitable pathway for regression analysis, the top 20% pathways regarding their variance in activity were chosen for the regression model to predict. Pathways with little variance were found to be better predicted by a null model. To factor in biological significance, the intersect of the 25 most significantly altered pathways from GSVA with the high variance pathways was computed. This resulted in three significantly altered and highly variant pathways among which the REAC-TOME_INTERLEUKIN_36_PATHWAY (IL-36 pathway) was selected. This gene set ranks 8th among the highest upregulated pathways with an associated p-value of 8.411155e-15. Interleukin 36 signaling is connected to both MAPK activity, through the activation of NF-κB and the expression of integrin alpha6beta4.(Bhatia *et al.*, 2013; Liberzon *et al.*, 2015b; Queen *et al.*, 2019).

Regression of the IL-36 pathway gene set showed mixed results. After multiple testing an architecture with two hidden layers with 10 and 20 neurons respectively at `set.seed(50)` was shown to produce the best results for neuronal network regression. Among the tested models, the neuronal network performed best on the test data with a mean squared error (MSE) of 0.06. However, the linear regression model failed to predict the data accurately (MSE = 0.62). Repeated linear regression with just pathways contributing significantly to the result, the performance was enhanced (MSE = 0.40), however, remained worse than a null model (MSE = 0.22) (Supplementary material figure 6.5). A comparison of the MSE on the test and training data revealed, that the linear model is highly overfitted (ΔMSE = +0.55) with the linear model with significant pathways fitting slightly better (ΔMSE = +0.23) to the data. Our null model displayed a good, yet slightly underfitted performance with ΔMSE = -0.08. With a ΔMSE = +0.009 the neuronal network shows an excellent fit.

A comparison of the four regression models via the F-test function `var.test()` showed a significant improvement in the neuronal network compared to all other models. All other models showed no significant differences in their performance compared to each other. (Supplementary material figure

6.5) From this data, we can conclude that a neuronal network is the best choice for most accurately predicting IL-36 pathway activity in our test data.

4 Discussion

Our pan-cancer analysis showed four clusters in pathway activity data. We were able to find specific pathways, which were enriched only in certain histological types like glioblastoma and adenocarcinoma. The focused analysis of THCA expression data revealed pathways driving carcinogenesis in Thyroid cancer. Furthermore, we were able to subcategorize THCA into three subtypes based on proliferative signaling pathway activity. As shown by the data signaling through alpha6beta4, RAS, JAK/STAT, and EWSR1/FLI1-fusion mediated pathways are linked to the non-follicular histological subtype of THCA.

Our findings from pan-cancer expression data show promising results. Via GSVA analysis, we identified four clusters in the cancer types correlating strongly to the associated histological type. Glioblastoma seem to take a special role as they are predominantly characterized by the high activity of neural crest differentiation pathways and receptor tyrosine kinases. This is in line with previous studies showing that glioblastoma derive from neural crest cells Jo *et al.* (2019).

Further, especially liver and kidney adenocarcinoma seemed to form a strong subcluster within other adenocarcinoma. They are characterized by exceptionally high activity of metabolic pathways such as carbohydrate metabolism, lipid, and amino acid synthesis. Again, this change in metabolism was previously found in hepatocellular carcinoma (Sangineto *et al.*, 2020). Upregulation of these metabolic pathways may lead to cell growth and proliferation, due to higher metabolic activity, providing more biomass and energy.

The most significant classification we found was the clustering of tumor types by their differentiation stage. Poorly differentiated tumors like leukemia and squamous cell carcinoma show an upregulation of pathways associated with embryonic stem cell-like expression signatures. In contrast, highly differentiated tumors like most adenocarcinoma as well as most glioblastoma show low activation of these gene sets. Such a clustering by differentiation stage was previously described by Ben-Porath *et al.*. However, these findings cannot be verified directly as provided annotation data did not contain information regarding the differentiation stage (Ben-Porath *et al.*, 2008).

From our GSEA and pan-cancer GSVA results, we identify two separate ways of carcinogenesis in THCA. The follicular subtype upregulates proliferative signaling through mTOR/PI3K and MAPK signaling pathways, which goes along with previous studies Noh *et al.* (2010).

The finding that the alpha6beta4 integrin signaling pathway and associated pathways such as IL-36 signaling and Typ I hemidesmosome synthesis were significantly enhanced in THCA is in line with previous studies. Those studies link alpha6beta4 signaling to the development of aggressive forms of thyroid cancer (Noh *et al.*, 2010; Queen *et al.*, 2019). Also, oncogenic signaling pathways commonly associated with different cancer types were significantly upregulated in THCAs. Among them, we observed ERBB2 and MST1 signaling commonly found in breast cancer. A role for MSP/Ron in breast

cancer has recently been elucidated, wherein this pathway regulates tumor growth, angiogenesis, and metastasis (Kretschmann *et al.*, 2010).

An important pathway upregulated in THCA is signaling through EWSR1/FLI1-fusion protein, while non-histone protein methylation is downregulated in THCA. This process was identified as an important modulator of intracellular signaling by the MAPK, WNT, BMP, Hippo, and JAK/STAT pathways and might play an important role as a driver of carcinogenesis in THCA (Biggar and Li, 2015). Together these findings give a general overview of mechanisms driving carcinogenesis in THCA. However, no information about possible THCA subtypes or differences in pathway activity between patients can be obtained from this data.

Pan-cancer GSVA shows three distinct clusters in the expression data, upregulating either one or both ways of proliferative signaling. While the follicular subtype seemed to strongly correlate with one cluster, a similar process was not observed in tall-cell and classical phenotypes. With more detailed annotation data it might be possible to link anaplastic and papillary histological subtypes of THCA to the two yet unassigned clusters.

Despite differences in proliferative signaling, all clusters share an upregulated hedgehog signaling pathway, which is consistent with the literature (Hinterseher *et al.*, 2014). Also, metabolic changes in line with the Warburg effect were observed in all clusters.

For regression analysis by linear regression and a neural network the IL-36 pathway was chosen since it is connected to both MAPK activity and integrin alpha6beta4 expression through the activation of NF-kB. An effective regression might be crucial in finding potentially druggable targets in combating THCA. Our data suggest that our neuronal network is well suited to predict pathway activities from GSEA data. The model shows an excellent fit to data and produces only minor errors. However, both linear models struggle in predicting the data accurately. This might be since GSEA pathway activity data usually clusters into an up- and downregulated group with no values in between. Since the IL-36 pathway also shows this problem, the two clusters might produce larger correlation values that might impact the accuracy of the regression coefficients and the intercept. Secondly, the correlation of the residuals with the test data values did not approach zero, thus, our linearity assumption is not met. Therefore, it can be concluded that a linear regression model is not well suited to predict the IL-36 pathway activity accurately.

Conclusion and Outlook

Taken together our results are in line with current research and allow for the following hypothesis: The expression profile of a given cancer type depends highly on its differentiation stage and its histological type but little on the actual tumor type itself. Understanding how these changes in expression link to mutational signatures might help in developing druggable targets for therapy.

Our findings suggest THCA can be divided into three subtypes based on which proliferative signaling pathway is active. These findings are in line with previous studies.

Further ways of analysis could be the prediction of the histological type of THCA as well as the way of carcinogenesis with a neuronal network. This might be possible with a larger training data set as well as more detailed and specified annotations. Furthermore, it might be possible to link

whole genome sequencing and methylation data to pathway activity. In that way, one could suggest a suitable targeted therapy option for a THCA patient based only on sequencing data from a small biopsy sample.

5 References

Alberts, J, B., and Walter, P (2015). Molecular biology of the cell, New York: Garland science.

Bednarczyk, JL, and McIntyre, BW (1992). Expression and ligand-binding function of the integrin alpha4beta1 (VLA-4) on neural-crest-derived tumor cell lines. Clinical & Experimental Metastasis 10, 281–290.

Ben-Porath, I, Thomson, MW, Carey, VJ, Ge, R, Bell, GW, Regev, A, and Weinberg, RA (2008). An embryonic stem cell-like gene expression signature in poorly differentiated aggressive human tumors. Nat Genet 40, 499–507.

Bhatia, V, Mula, RV, and Falzon, M (2013). Parathyroid hormone-related protein regulates integrin alpha6 and beta4 levels via transcriptional and post-translational pathways. Exp Cell Res 319, 1419–1430.

Bi, C-L, Zhang, Y-Q, Li, B, Guo, M, and Fu, Y-L (2019). Retracted: MicroRNA-520a-3p suppresses epithelial–mesenchymal transition, invasion, and migration of papillary thyroid carcinoma cells via the JAK1-mediated JAK/STAT signaling pathway. Journal of Cellular Physiology 234, 4054–4067.

Biggar, KK, and Li, SSC (2015). Non-histone protein methylation as a regulator of cellular signalling and function. Nature Reviews Molecular Cell Biology 16, 5–17.

Cabanillas, ME, McFadden, DG, and Durante, C (2016). Thyroid cancer. Lancet 388, 2783–2795.

Coca-Pelaz, A et al. (2020). Papillary thyroid cancer-aggressive variants and impact on management: A narrative review. Adv Ther 37, 3112–3128.

Durinck, S, Spellman, PT, Birney, E, and Huber, W (2009). Mapping identifiers for the integration of genomic datasets with the r/bioconductor package biomaRt. Nature Protocols 4, 1184–1191.

Fritsch, S, Guenther, F, and Wright, MN (2019). Neuralnet: Training of neural networks.

Furuya, F, Lu, C, Willingham, MC, and Cheng, S (2007). Inhibition of phosphatidylinositol 3-kinase delays tumor progression and blocks metastatic spread in a mouse model of thyroid cancer. Carcinogenesis 28, 2451–2458.

Hanahan, D, and Weinberg, RA (2011). Hallmarks of cancer: The next generation. Cell 144, 646–674.

Hänzelmann, S, Castelo, R, and Guinney, J (2013a). GSVA: Gene set variation analysis for microarray and RNA-seq data. BMC Bioinformatics 14, 7.

Hänzelmann, S, Castelo, R, and Guinney, J (2013b). GSVA: Gene set variation analysis for microarray and RNA-Seq data. BMC Bioinformatics.

Hao, Y et al. (2021). Integrated analysis of multimodal single-cell data. Cell 184, 3573–3587.e29.

Hinterseher, U, Wunderlich, A, Roth, S, Ramaswamy, A, Bartsch, DK, Hauptmann, S, Greene, BH, Fendrich, V, and Hoffmann, S (2014). Expression of hedgehog signalling pathway in anaplastic thyroid cancer. Endocrine 45, 439–447.

Jo, DH, Kim, JH, and Kim, JH (2019). Targeting tyrosine kinases for treatment of ocular tumors. Archives of Pharmacal Research 42, 305–318.

Kant, R, Davis, A, and Verma, V (2020). Thyroid nodules: Advances in evaluation and management. Am Fam Physician 102, 298–304.

Konopka, T (2022). Umap: Uniform manifold approximation and projection.

Korotkevich, G, Sukhov, V, and Sergushichev, A (2019). Fast gene set enrichment analysis. bioRxiv.

Kretschmann, KL, Eyob, H, Buys, SS, and Welm, AL (2010). The macrophage stimulating protein/ron pathway as a potential therapeutic target to impede multiple mechanisms involved in breast cancer progression. Curr Drug Targets 11, 1157–1168.

Liberzon, A, Birger, C, Thorvaldsdóttir, H, Ghandi, M, Mesirov, JP, and Tamayo, P (2015b). The molecular signatures database (MSigDB) hallmark gene set collection. Cell Syst 1, 417–425.

Liberzon, A, Birger, C, Thorvaldsdóttir, H, Ghandi, M, Mesirov, JP, and Tamayo, P (2015a). The molecular signatures database (MSigDB) hallmark gene set collection. Cell Syst 1, 417–425.

Lin, JD (2007). Papillary thyroid carcinoma with lymph node metastases. Growth Factors 25, 41–49.

Lunt, M (2013). Introduction to statistical modelling: Linear regression. Rheumatology 54, 1137–1140.

Maaten, L van der, and Hinton, G (2008). Visualizing data using t-SNE. Journal of Machine Learning Research 9, 2579–2605.

Noh, TW, Soung, YH, Kim, HI, Gil, HJ, Kim, JM, Lee, EJ, and Chung, J (2010). Effect of beta4 integrin knockdown by RNA interference in anaplastic thyroid carcinoma. Anticancer Res 30, 4485–4492.

Oliveira, G, Polónia, A, Cameselle-Teijeiro, JM, Leitão, D, Sapia, S, Sobrinho-Simões, M, and Eloy, C (2017). EWSR1 rearrangement is a frequent event in papillary thyroid carcinoma and in carcinoma of the thyroid with ewing family tumor elements (CEFTE). Virchows Archiv 470, 517–525.

Queen, D, Ediriweera, C, and Liu, L (2019). Function and regulation of IL-36 signaling in inflammatory diseases and cancer development. Front Cell Dev Biol 7, 317.

Rabinovitz, I, and Mercurio, AM (1996). The integrin alpha 6 beta 4 and the biology of carcinoma. Biochem Cell Biol 74, 811–821.

Reese, A (2019). Modern statistics for modern biology s. HolmesW. Huber 2019 cambridge cambridge university press xxiv + 382 pp., £ 49.99 ISBN 978-1-108-70529-5. Journal of the Royal Statistical Society: Series A (Statistics in Society) 182, 1647–1647.

Riedmiller, MA Rprop - description and implementation details.

Sangineto, M, Villani, R, Cavallone, F, Romano, A, Loizzi, D, and Serviddio, G (2020). Lipid metabolism in development and progression of hepatocellular carcinoma. Cancers 12, 1419.

Sharma, S, Quinn, D, Melenhorst, JJ, and Pruteanu-Malinici, I (2021). High-dimensional immune monitoring for chimeric antigen receptor t cell therapies. Current Hematologic Malignancy Reports 16, 112–116.

Subramanian, A et al. (2005). Gene set enrichment analysis: A knowledge-based approach for interpreting genome-wide expression profiles. Proc Natl Acad Sci U S A 102, 15545–15550.

Wade, A, Robinson, AE, Engler, JR, Petritsch, C, James, CD, and Phillips, JJ (2013). Proteoglycans and their roles in brain cancer. The FEBS Journal 280, 2399–2417.

Wang, X, Pei, Z, Hossain, A, Bai, Y, and Chen, G (2021). Transcription factor-based gene therapy to treat glioblastoma through direct neuronal conversion. Cancer Biol Med 18, 860–874.

Wickham, H (2016). ggplot2: Elegant graphics for data analysis, Springer-Verlag New York.

Zyla, J, Marczyk, M, Weiner, J, and Polanska, J (2017). Ranking metrics in gene set enrichment analysis: Do they matter? BMC Bioinformatics 18, 256.

6 Supplementary material

6.1 Given data

For pan-cancer analysis, a gene expression data frame with normalized and log2 transformed bulk RNA-seq expression data for 60,489 genes in 9741 patients with 33 different forms of cancer and clinical annotations was used. The data was derived from The Cancer Genome Atlas (TCGA). For the focused analysis, only THCA data consisting of three data frames was used: The first two contain normalized, and log2 transformed bulk RNA-seq expression data for 19,624 genes in 59 THCA patients for carcinogenic and homeostatic tissue. The third data frame complements the data with the respective clinical annotations. The last object contains 46 pathways associated with the hallmarks of cancer in the form of a list of vectors containing gene identifiers. To perform enrichment analysis, all 6366 canonical pathways were selected from the Molecular Signatures Database (MSigDB) (Liberzon *et al.*, 2015b) with the `msigdbr::msigdbr()` function. As not to introduce a bias during enrichment analysis, the similarity of MSigDB pathways among themselves as well as with the hallmark pathways was computed with the Jaccard index. The pathways with a Jaccard index greater than a set threshold were discarded.

6.2 Preprocessing of expression data

All expression data were checked for missing values. Subsequently, low variance filtering was performed for TCGA and THCA tumor expression data. Genes with variances below a threshold were discarded to reduce dimensionality. Next, biotype filtering was performed for pan-cancer and THCA expression data to reduce dimensionality further. Only genes sharing biotypes with the hallmark pathways were kept for the following analysis. The biotypes of the genes were retrieved using the `biomart::getBM()` function from the "biomart" package (Durinck *et al.*, 2009). Only MSigDB pathways in which over 99% of their respective genes were present in the filtered expression data were selected as final pathways.

6.3 Additional Computational Methods

A Principal component analysis (PCA) is used to alter the coordinates of a given dataset to its eigenvectors. This matrix rotation results in a new set of basis vectors called principal components (PCs) - the eigenvectors - that are orthogonal and show little correlation. Sorting the PCs by their associated eigenvalue, the PCs explaining the most variance can easily be identified, as they have the highest eigenvalue. By displaying the data set in a coordinate system span by the n most variant PCs, the dimensionalty of the data set is reduced to $\mathbb{R}^n$ with the lowest loss in variance. (Reese, 2019)

Linear regression is a statistical model that uses measurable values to predict an outcome. For this purpose, a linear function serves as basis to build the linear regression equation (Lunt, 2013). The coefficients for each variable are estimated by their correlation and slope with the predicted parameter.

Lastly, all coefficients as well as the intersect are optimized for the data set with a least sum of squares method.

The Jaccard index is the intersection, divided by the union of two sets. Therefore, it can be used to identify the similarity of the sets.

6.4 Packages

Table 6.1: Packages used in the analysis.

| Package	Usage	Authors
biomart	renaming genenames to ensembleIDs	Durinck *et al.,* 2009
msigdbr	downloading canonical pathways and included genes from MSigDB	Bhuva *et al.,* 2022
dplyr	editing of dataframes	Wickham *et al.,* 2022
ggplot2	creation of plots with detailed options	Wickham *et al.,* 2022
pheatmap	creation of heatmaps with detailed options	Kolde, 2019
vioplot	creation of violinplots	Kolde, 2019
VennDiagram	creation of VENN-diagrams	Chen, 2022
fgsea	performing a GSEA	Korotkevich *et al.,* 2019
GSVA	performing a GSVA	Hänzelmann *et al.,* 2013
Complex Heatmap	creation of heatmaps with detailed options	Gu *et al.,* 2016
metaplot	creating of data-driven plots	Bergsma, 2019
gridExtra	implementing of "grid" graphics	Auguie and Antonov, 2017
umap	creating UMAPs	Konopka, 2022
gage	application of GSEA	Luo *et al.,* 2009
psych	performing an iterative factor analysis	Revelle, 2022
cluster	performing a cluster analysis	Maechler *et al.,* 2022
MASS	implementing of neural network	Ripley *et al.,* 2022
neuralnet	training of neural networks	Fritsch *et al.,* 2019
AnnotationDbi	translating ensemble ids into gennames	Pagès *et al.,* 2022
org.Hs.eg.db	translating ensemble ids into gennames	Carlson, 2019

6.5 Additional Figures
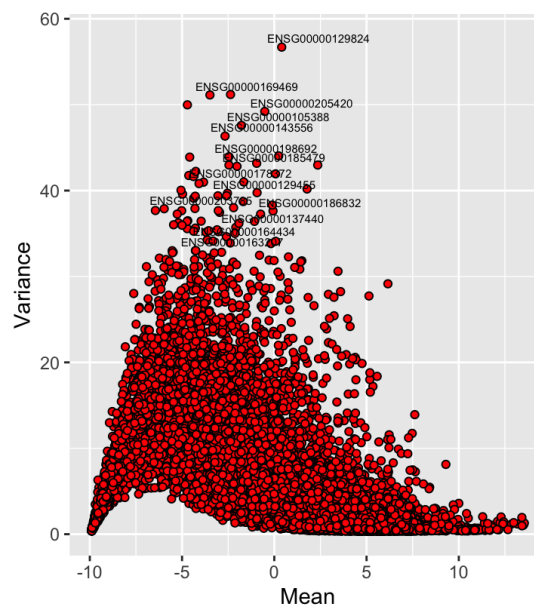
Figure 6.1: Mean-variance plot of cleaned TCGA expression data. y-axis shows variance of a gene expression, x-axis shows the log2 mean of a gene expression. Genes with variance greater 33 are labelled with their EnsemblID
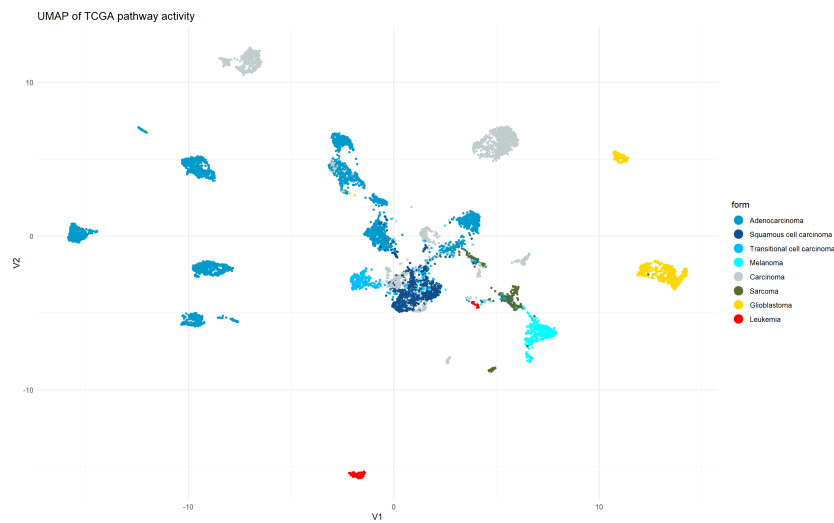

Figure 6.2: UMAP of TCGA pathway activity, colored by histological type

Figure 6.3: Pathway activity of the 100 most variant pathways for each patient. Column and row clusters were obtained by complete hierachical clustering. Pathway activities were computed via GSVA of pan-cancer expression data.
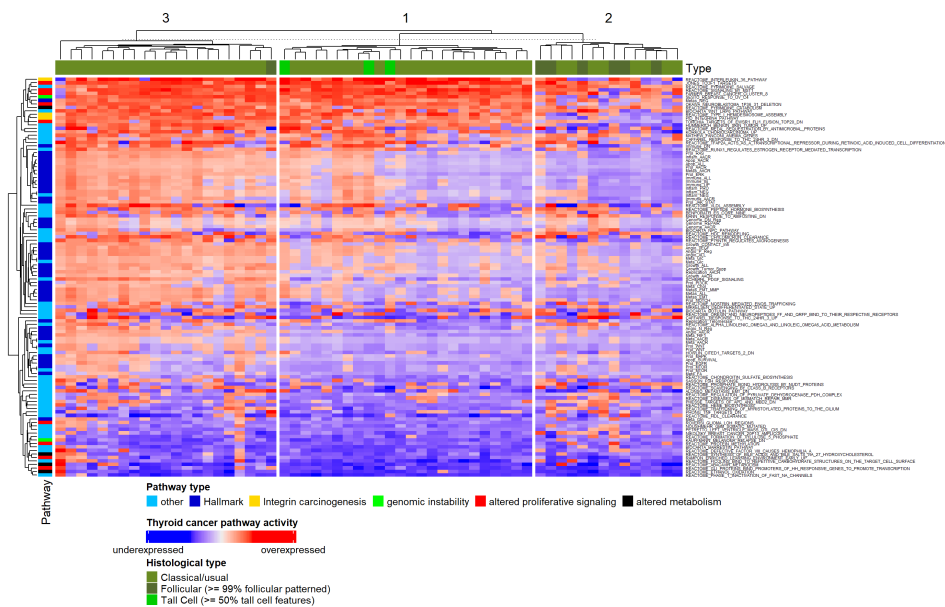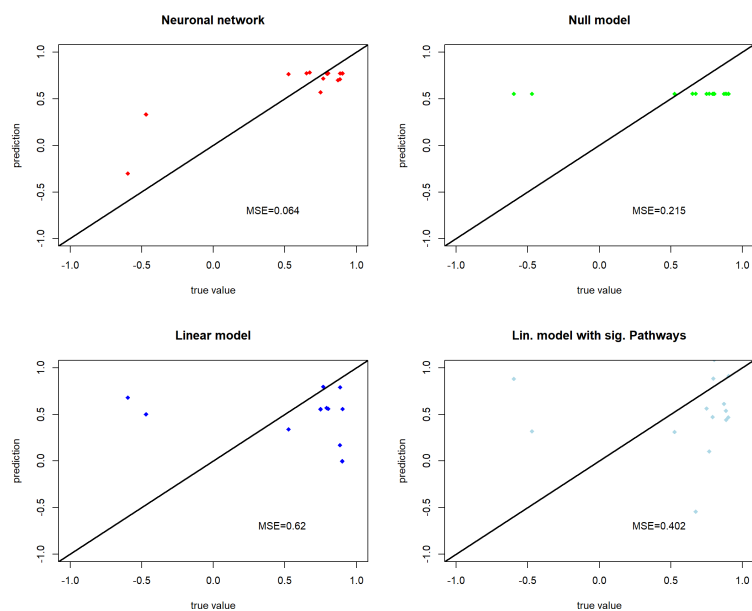

Figure 6.4: Pathway activity of the 50 most variant, hallmark, and 20 most significantly altered pathways for each patient. Column clusters were obtained by k-means clustering with k=3. Pathway activities were computed via GSEA of THCA expression data.
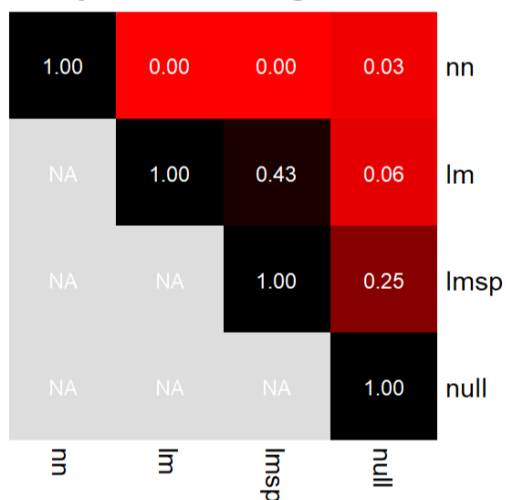
Figure 6.5: Regression results for various models on THCA GSEA test data. True values are plotted against predicted values, black slope indicate a perfect prediction. p-values are obtained from a two-sided variance test and displayed as heatmap. nn = neuronal network, lm = linear regression, lmsp = linear regression with only significant pathways, null = null model.